

Preparation and magnetic properties of nanosized amorphous ternary Fe–Ni–Co alloy powders

Kurikka V.P.M. Shafi and Aharon Gedanken^{a)}

Department of Chemistry, Bar-Ilan University, Ramat-Gan 52900, Israel

Ruslan Prozorov

Department of Physics, Bar-Ilan University, Ramat-Gan 52900, Israel

Adam Revesz and Janos Lendvai

Department of General Physics, Lorand Eotvos University, H-1088, Budapest, Hungary

(Received 1 August 1999; accepted 29 October 1999)

Nanosized amorphous alloy powders of Fe₂₅Ni₁₃Co₆₂, Fe₃₈Ni₂₃Co₃₉, Fe₄₀Ni₂₄Co₃₆, and Fe₆₉Ni₉Co₂₂ were prepared by sonochemical decomposition of solutions of volatile organic precursors, Fe(CO)₅, Ni(CO)₄, and Co(NO)(CO)₃ in decalin, under an argon pressure of 100 to 150 kPa at 273 K. The amorphous nature of these particles was confirmed by various techniques, such as scanning electron microscopy, transmission electron microscopy, electron microdiffraction, and x-ray diffractograms. Magnetic measurements indicated that the as-prepared amorphous Fe–Ni–Co alloy particles were superparamagnetic. The observed magnetization measured up to a field of 1.5 kG of the annealed Fe–Ni–Co samples (75–87 emu g⁻¹) was significantly lower than that for the reported multidomain bulk particles (175 emu g⁻¹), reflecting the ultrafine nature of our sample.

I. INTRODUCTION

Amorphous alloys—metallic glasses or glassy metals obtained by rapid quenching of the melt—lack the long-range atomic order of their crystalline counterparts. The unique electronic, magnetic, and corrosion-resistant properties,^{1–4} make these systems technologically important. For example, the ferromagnetic amorphous alloys containing Fe and Co have excellent soft magnetic properties equivalent or superior to those of conventional materials and are being used in magnetic storage media and power transformer cores.⁵ The high resistivity of the amorphous alloys, generally 2 to 4 times larger than the corresponding transition metal crystalline alloys, results in a smaller eddy current contribution to the permeability and losses, which is very important at higher frequency device applications.⁶

Transition metal alloys with a wide variety of metalloids, such as transition metal–metalloid alloys (TM-M) and rare earth–transition metal (RE-TM) alloys, have been reported, the TM-M alloys typically contain about 80 at.% Fe, Co, Ni with the remainder being B, C, Si, P, or Al as glass formers. The use of glass former is to lower

the melting point, thus making it possible to quench the alloy through its glass temperature rapidly enough to form the amorphous phase. Although these metalloids stabilize the amorphous phase, their presence drastically alters the magnetic properties of the alloys. The electron donated to the *d* band changes the electronic environment and thus lowers the saturation magnetization (M_s) and Curie temperature (T_c).⁵

Soft magnetic alloys with high-saturation magnetization, reduced magnetocrystalline anisotropy, and zero magnetostriction, are the technologically important magnetic materials.^{7,8} An Fe–Ni–Co alloy system is particularly interesting as many compositions with zero magnetostriction are known in this system. The Perm and the Super Invar properties of some of the Fe–Ni–Co alloys, coupled with the dependence of magnetic and mechanical properties on the $\alpha \leftrightarrow \gamma$ martensitic structural transformations of it, make this system a versatile one for technological applications.^{9,10}

To our knowledge, no amorphous Fe–Ni–Co ternary alloy system without any glass former (metalloid), has been reported so far in the literature. Recently, Ishio *et al.*¹¹ have studied the magnetostrictive properties of Co_xFe_yNi_z alloy system ($0.9 \geq x \geq 0.4$, $0.5 \geq y \geq 0.15$, and $0.4 \geq z$) in the composition region of the face-centered-cubic (γ) phase. Magnetostriction and magneto-resistance in the Fe–Ni–Co ternary alloy system have also been examined by Miyazaki *et al.*^{12,13} Magnetic

^{a)}Address all correspondence to this author.
e-mail: gedanken@mail.biu.ac.il

properties and the $\alpha \leftrightarrow \gamma$ martensitic structural transformations have been investigated by Achilleos *et al.*¹⁴ and others.¹⁵

The chemical effect of ultrasound does not originate from a direct coupling with molecular vibrations but from a nonlinear phenomenon called cavitation, which involves the formation, growth, and subsequent implosive collapse of a bubble in a liquid. Acoustic cavitation generates a transient localized hot spot with an effective temperature of 5000 K and a submicrosecond collapse time.^{16–18} The rapid cavitation cooling rate ($>10^9$ K s⁻¹) is much higher than that obtained by the conventional melt-spinning¹⁹ (10^5 to 10^6 K s⁻¹) technique used to prepare amorphous materials. We have explored this cavitation phenomenon to prepare the amorphous metals,²⁰ alloys,^{21,22} oxides,²³ and ferrites.^{24,25} Here we discuss the sonochemical synthesis and characterization of nanosized amorphous Fe–Ni–Co particles. This is a continuation of our work on the bimetallic metal alloys Co–Ni reported earlier in this journal.²²

II. EXPERIMENTAL

The Fe–Ni–Co alloy was prepared by our previously published method for Co–Ni alloys²² by ultrasonic irradiation of the solution of Fe(CO)₅, Co(NO)(CO)₃ and Ni(CO)₄ in decane at 273 K under 100 to 150 kPa (1 to 1.5 atm) of argon, with a high-intensity ultrasonic probe (Sonics and Materials, model VC-600) (1.25-cm Ti horn, 20 kHz, 100 W cm⁻²). The various compositions of Fe–Ni–Co (Fe₂₅Ni₁₃Co₆₂, Fe₃₈Ni₂₃Co₃₉, Fe₄₀Ni₂₄Co₃₆, Fe₆₉Ni₉Co₂₂) were prepared by varying the molar concentration of the precursors in solution.

Powder x-ray diffractograms were recorded on a Rigaku x-ray diffractometer (Cu K α radiation, $\lambda = 0.15418$ nm). Scanning electron micrographs and energy dispersive x-ray analysis (EDX) were carried out on a JEOL-JSM-840 electron microscope. Transmission electron micrographs were obtained with a JEOL-JEM100SX electron microscope. Magnetization loops were measured at room temperature with an Oxford Instrument vibrating sample magnetometer. Surface area [Brunauer–Emmett–Teller (BET) method] was measured on a Micromeritics–Gemini surface area analyzer. Differential scanning calorimetry (DSC) thermograms were obtained on a Mettler-Toledo DSC 25 calorimeter at a heating rate of 10 °C/min under flowing pure argon (50 ml/min). Elemental analyses were carried out on an EA 1110 CHNS-O analyzer. All sample preparation and transfer for these measurements were done inside a glove box.

III. RESULTS AND DISCUSSION

Alloy compositions were determined by elemental and energy-dispersive x-ray analyses. The EDX profile of a representative sample, Fe₆₉Ni₉Co₂₂, is shown in Fig. 1.

Because the atomic numbers of Fe, Ni, and Co are close to each other, the alloy composition was estimated from the ratio of the x-ray emission intensities from these elements. The x-ray intensity was not corrected for absorption and fluorescence effects as these particles were much smaller than the free path for x-ray transmission through solids (i.e., 100 nm).

The elemental analyses of the as-prepared samples show that the amorphous alloy powders have over 95% metal by mass, with small amounts of carbon (<3%) and oxygen (<2%). The presence of carbon and oxygen is presumably a result of the decomposition of alkane solvents during ultrasonication or adsorbed CO. The infrared spectra of the as-prepared samples showed peaks at 2100 cm⁻¹ characteristic of adsorbed CO molecules on the surface. These impurities probably play an important role in stabilizing the amorphous structure of the samples.²¹ Further the analyses of the annealed samples (heated at 300 °C under high pure Ar for 10 h) showed only <0.5% of C, H, and O, and this indicated that the adsorbed surface impurities were almost completely removed.

Electron microdiffraction and x-ray diffraction techniques confirm the amorphous nature of the alloy particles. The transmission electron microscope (TEM) image (Fig. 2) of the as-prepared Fe₃₈Ni₂₃Co₃₉ sample shows the alloy powders as agglomerates of small particles with overall diameters of <10 nm. The exact size of the particle is difficult to determine as most of the particles are aggregated in a spongelike form. The TEM microdiffraction [Fig. 2(a) inset] of the alloy particles shows only diffuse rings characteristic of amorphous materials. The other as-prepared samples behave in a similar fashion. The TEM micrograph of the annealed Fe₃₈Ni₂₃Co₃₉ sample (heated at 500 °C for 5 h under Ar) is shown in Fig. 3. Uniform near-spherical particles of <10 nm can be seen in this micrograph. The x-ray diffraction pattern for the as-prepared sample as well as the annealed samples of Fe₂₅Ni₁₃Co₆₂ and Fe₆₉Ni₉Co₂₂

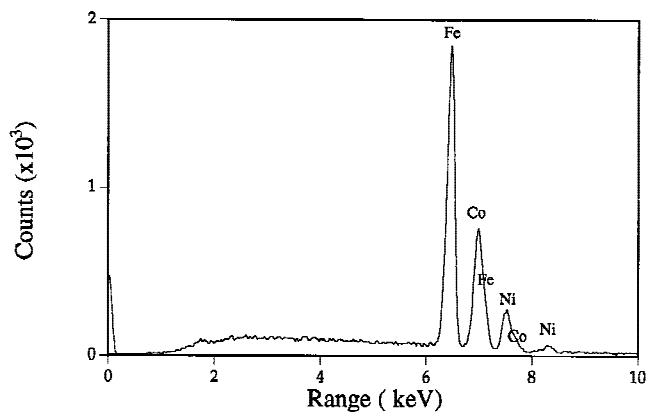


FIG. 1. EDX profiles for annealed Fe₆₉Ni₉Co₂₂ alloy sample.

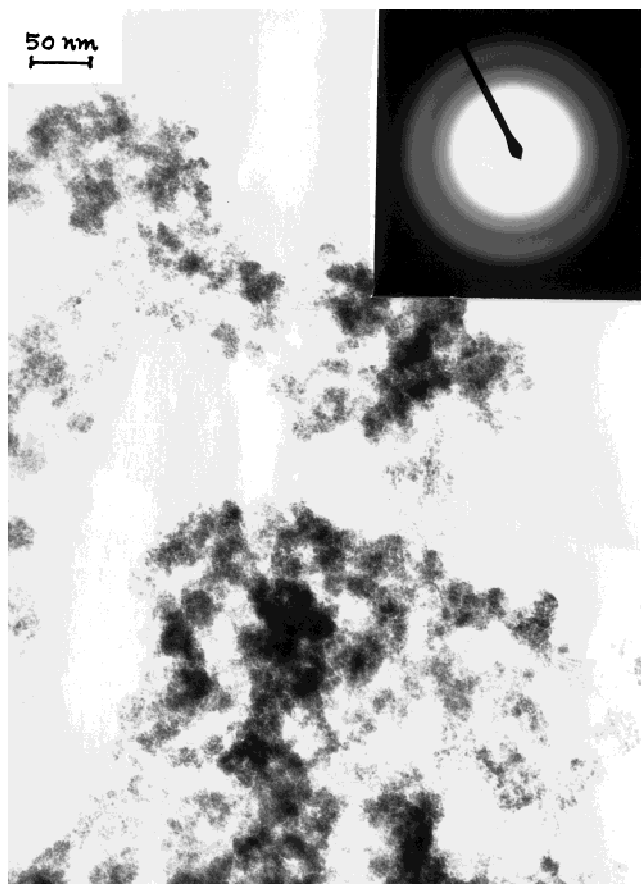


FIG. 2. TEM image of amorphous Fe₃₈Ni₂₃Co₃₉ with microdiffraction patterns (inset).

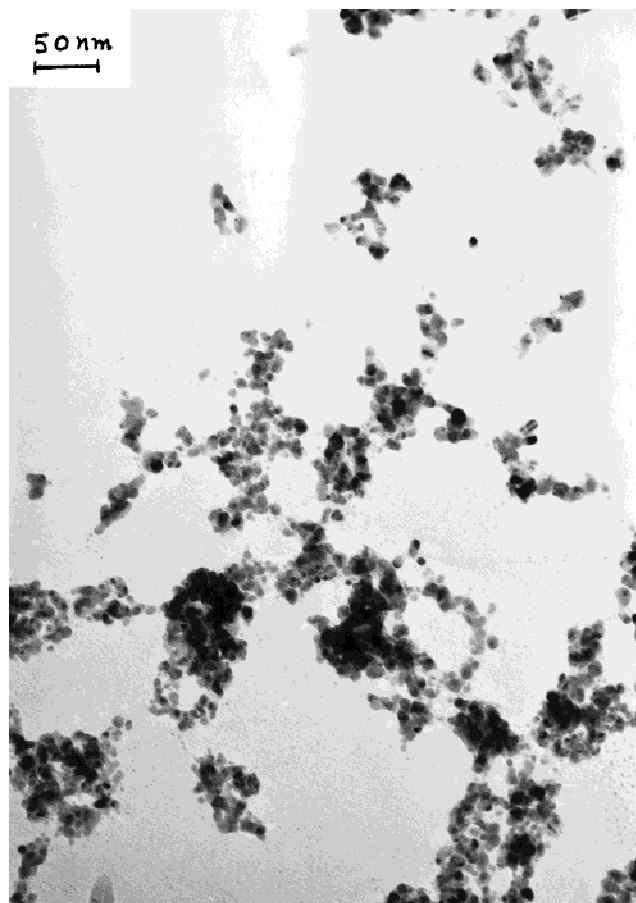


FIG. 3. TEM image of annealed Fe₃₈Ni₂₃Co₃₉ alloy sample.

(heat treated under pure argon at 500 °C for 5 h) are shown in Fig. 4. The as-prepared amorphous sample [Fig. 4(a)] shows no sharp diffraction pattern indicating the amorphous nature. The pattern for the Fe₆₉Ni₉Co₂₂ sample shows peaks characteristic of the α -phase as well as the γ -phase, while the pattern for Fe₂₅Ni₁₃Co₆₂ shows peaks predominantly of the γ -phase. The γ -phase is of the Fe–Ni type in the disordered state and the α -phase is that of the Fe–Co alloy system. The existence of both α - and γ -phases in the annealed samples is due to the $\alpha \leftrightarrow \gamma$ martensitic structural transformations. The alloy systems Fe₃₈Ni₂₃Co₃₉, Fe₂₅Ni₁₃Co₆₂, and Fe₄₀Ni₂₄Co₃₆ lie at the boundary of the α - and the γ -phase, while the system Fe₆₉Ni₉Co₂₂ is in the α -region of the phase diagram of the ternary Fe–Ni–Co system.¹² The magnetization curve of the amorphous sample Fe₆₉Ni₉Co₂₂ measured at room temperature (Fig. 5) does not reach saturation even at a magnetic field of 15 kG, and no hysteresis is found, indicating that the as-prepared (amorphous) Fe–Ni–Co particles are superparamagnetic. Other samples behave similarly. Figure 6 shows the magnetization curves of the annealed samples of Fe–Ni–Co alloys. (The scale in Fig. 6 is larger than that in Fig. 5 because of the crystalline nature of the compound.) The

magnetic properties of the various compositions of the alloy particles are given in Table I. The observed values of magnetization of the annealed samples, 77–87 emu g⁻¹ at high enough field of 15 kG, are significantly lower than that for the reported¹⁵ multidomain Fe–Ni–Co particles (175–180 emu g⁻¹), and this reflects the ultrafine nature of our sample. Specifically, the difference in the magnetization value between the bulk and our nanosized materials can be attributed to the small particle size effect. This can be readily seen from the high surface area of our annealed samples (i.e., 25–35 m²/g) and the small particle sizes (10–15 nm) estimated from broadening of x-ray lines with the Scherrer equation (see Table I). The decrease in surface area of the heated sample is due to the increase in particle size by sintering. It is known that the magnetic properties, like saturation magnetization and hyperfine field value, of nanoparticles are much smaller than those of the corresponding bulk materials.^{22,24–28} Because the energy of a magnetic particle in an external field is proportional to its volume (via the number of magnetic molecules), it decreases as the cube of the linear particle dimension. When this energy becomes comparable to kT , thermal fluctuations will significantly reduce the total magnetic moment at a given field. The

large surface-to-volume ratio for small particles can also lead to decreased magnetization values. The magnetic molecules on the surface lack complete coordination. Finally, antiferromagnetic impurities like oxide and carbide can also decrease the total magnetization. Adsorbed carbonyl on amorphous materials can lead to metal carbide or oxide during sonication or the heating process.²⁹

The DSC curves of the as-prepared amorphous Fe–Ni–Co samples are shown in Fig. 7. Wide endothermic peaks below 300 °C in all the samples are due to desorption of adsorbed carbonyl and hydrocarbon solvent impurities. These peaks vanish in the successive runs of the DSC and this indicates the desorption endotherms of the adsorbed surface impurities. The crystallization behavior of the samples are different. The Fe₆₉Ni₉Co₂₂ sample [Fig. 7(a)] shows a wide exothermic peak centered around 310 °C. In the Fe₄₀Ni₂₄Co₃₆ sample [Fig. 7(b)] two exothermic peaks are detected, one at 370 and another at 400 °C, respectively. However, in the Fe₂₅Ni₁₃Co₆₂ sample [Fig. 7(c)], the sharp exothermic peak is at 370 °C and is immediately followed by another sharp endotherm at 390 °C. The crystallization peak of the Fe₃₈Ni₂₃Co₃₉ sample [Fig. 7(d)] is a sharp one at 365 °C and no endotherm is detected afterward. These

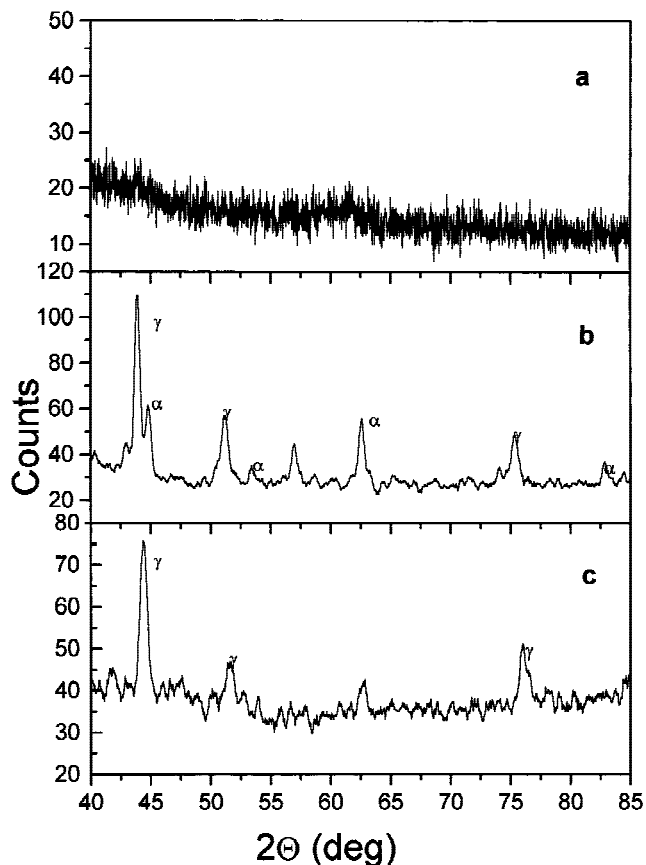


FIG. 4. XRD patterns for (a) amorphous Fe₂₅Ni₁₃Co₆₂, (b) annealed Fe₆₉Ni₉Co₂₂ sample, and (c) annealed Fe₂₅Ni₁₃Co₆₂ sample.

exo- and endothermic peaks completely vanish in the successive run, showing the irreversible nature of the transition. Further, we have examined the DSC curve of Fe₂₅Ni₁₃Co₆₂ sample, after annealing at 300 °C for 5 h to remove completely the surface adsorbed impurities, to check the possible role of the contaminants on the endotherm at 390 °C. The endothermic peak is still seen on the DSC curve even though shifted to 400 °C. From these

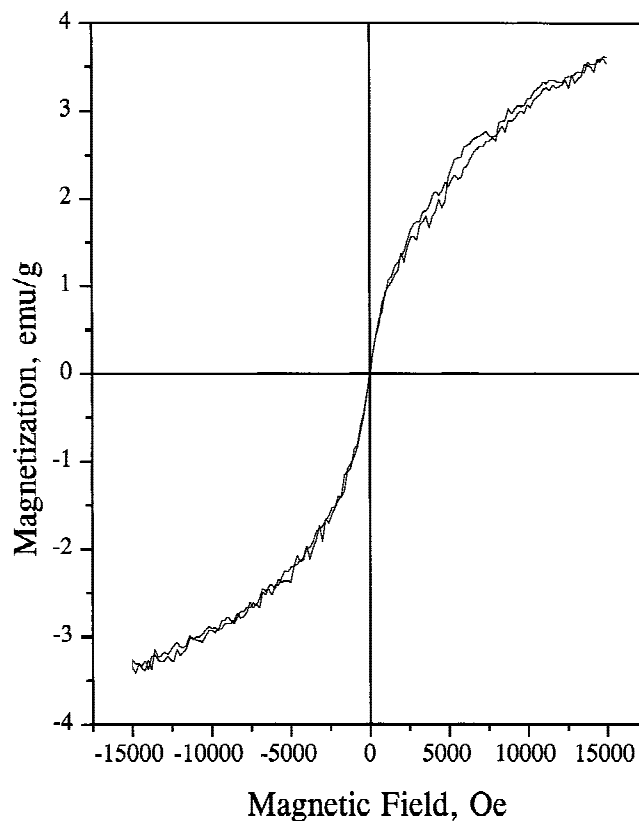


FIG. 5. Room-temperature magnetization curves of amorphous Fe₆₉Ni₉Co₂₂ sample.

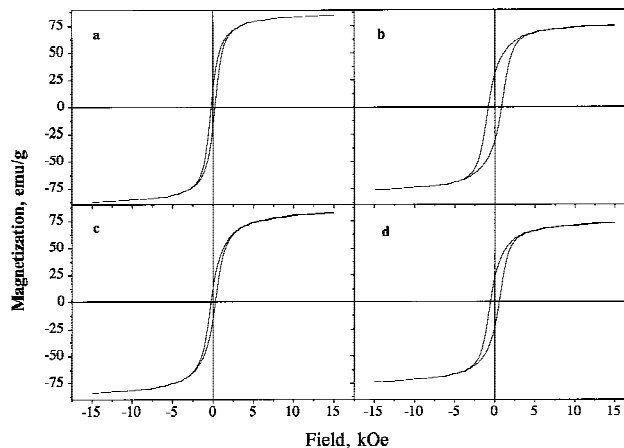
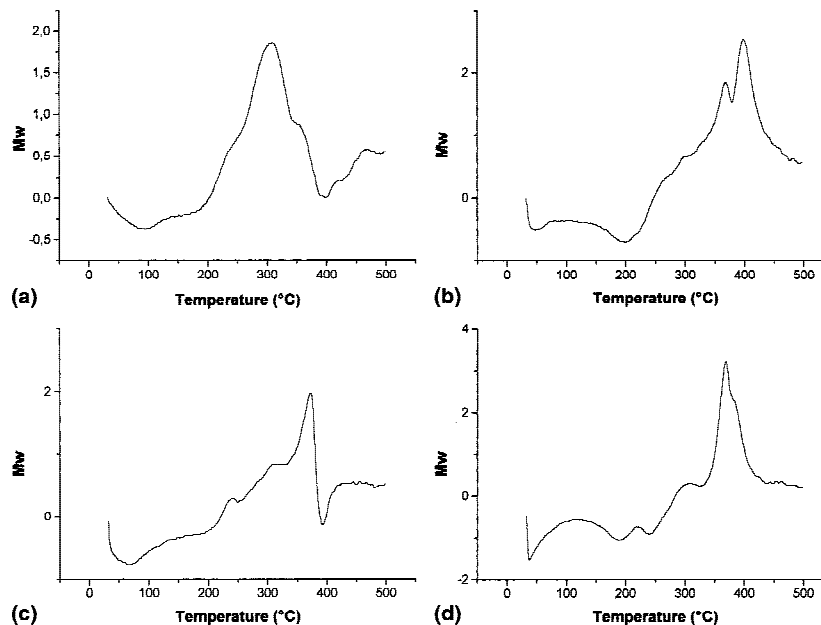


FIG. 6. Room-temperature magnetization curves of annealed Fe–Ni–Co samples: (a) Fe₃₈Ni₂₃Co₃₉, (b) Fe₂₅Ni₁₃Co₆₂, (c) Fe₆₉Ni₉Co₂₂, and (d) Fe₄₀Ni₂₄Co₃₆.

TABLE I. Compositions and magnetic properties of annealed alloy samples.

	Fe (at.%)	Ni (at.%)	Co (at.%)	Pseudobinary type	M_s (emu/g)	M_r (emu/g)	H_c (G)	Surface area (m ² /g)	Size (nm)
1	24.75	13.16	62.09	(Fe _{0.65} Ni _{0.35}) ₃₈ Co ₂	77.00	31.00	814	33	11.2
2	37.82	22.73	39.45	(Fe _{0.62} Ni _{0.38}) ₆₁ Co ₃₉	87.00	17.00	230	25	15.4
3	40.22	23.65	36.13	(Fe _{0.63} Ni _{0.37}) ₆₄ Co ₃₆	75.00	23.00	550	35	10.5
4	69.15	9.16	21.69	Fe ₆₉ Ni ₉ Co ₂₂	83.00	14.00	260	28	13.9

FIG. 7. DSC curve of amorphous samples: (a) Fe₆₉Ni₉Co₂₂, (b) Fe₄₀Ni₂₄Co₃₆, (c) Fe₂₅Ni₁₃Co₆₂, and (d) Fe₃₈Ni₂₃Co₃₉.

observations, we believe that the endotherms following the crystallization exotherms of the Fe–Ni–Co samples have to do with some kind of magnetic phase transition, the nature of which is not clear now. Systematic and detailed studies, like thermomagnetometry (TM) and variable temperature x-ray diffraction, are required to study this transition.

IV. CONCLUSIONS

Sonochemical decomposition of the solutions of volatile organic precursors Fe(CO)₅, Co(NO)(CO)₃, and Ni(CO)₄ in decalin at 273 K, under an argon pressure of 100 to 150 kPa (1 to 1.5 atm), yield amorphous, nanosized Fe–Ni–Co alloy particles. The composition of these alloy particles can be controlled by varying the initial precursor concentration in solution. Magnetic data indicate the superparamagnetic nature of the as-prepared amorphous sample and also the ultrafine nature of the crystallized sample.

ACKNOWLEDGMENTS

This research was supported by Grant No. 94-00230 from the US–Israel Binational Science Foundation (BSF), Jerusalem, Israel. We thank the Ministry of Sci-

ence & Arts for the Binational Indo-Israel Grant as well as the Hungary–Israel exchange scientist program. A. Gedanken is grateful to the Bar-Ilan Research Authorities for supporting this project. R. Prozorov acknowledges support from the Clore Foundations. We thank Prof. M. Deutsch for use of x-ray diffraction facilities and Prof. Y. Yeshurun for extending the facilities of the National Center for Magnetic Measurements at the Department of Physics, Bar-Ilan University.

REFERENCES

1. T.R. Anantharaman, *Materials Science Surveys, No. 2: Metallic Glasses*, edited by T.R. Anantharaman (Trans Tech Publications, Rockport, MA, 1984).
2. P. Haasen and R.I. Jaffe, *Amorphous Metals and Semiconductors* (Pergamon, London, 1986).
3. N.F. Motte and E.A. Davis, *Electronic Processes in Non-Crystalline Materials* (Clarendon Press, Oxford, 1979).
4. H. Steeb and H. Warlimont, *Rapidly Quenched Metals* (Elsevier, Amsterdam, 1985).
5. T. Egami, *Report Prog. Phys.* **47**, 1601 (1984).
6. F.E. Luborsky, in *Ferromagnetic Materials*, edited by E.P. Wohlfarth (North-Holland, Amsterdam, 1980), Vol. 1, p. 474.
7. C. Heck, *Magnetic Materials and Their Applications* (Butterworths, London, 1974).
8. S. Chikazumi and C.D. Graham, *Magnetism and Metallurgy* (Academic Press, New York, 1969).

9. M. Moronziski, *Physics and Applications of Invar Alloys*, Honda Memorial Series on Material Science Vol. 3 (Maruzen, Tokyo, 1978).
10. C. Connors and S.F. Jacobs, *J. Appl. Opt.* **22**, 1794 (1983).
11. S. Ishio, T. Kobayashi, S. Sugawara, and S. Kadowaki, *J. Magn. Mater.* **164**, 208 (1994).
12. T. Miyazaki and M. Oikawa, *J. Mag. Magn. Mater.* **97**, 171 (1991).
13. T. Miyazaki, T. Oomori, F. Sato, S. Ishio, and M. Oikawa, *J. Magn. Mater.* **129**, L135 (1994).
14. C.A. Achilleos, I.M. Kyprinidis, and I.A. Tsoukalas, *Solid State Commun.* **79**, 209 (1991).
15. D.A. Colling, *J. Appl. Phys.* **41**, 1038 (1970).
16. K.S. Suslick, *Science* **247**, 1439 (1990).
17. E.B. Flint and K.S. Suslick, *Science* **253**, 1397 (1991).
18. A.A. Atchley and L.A. Crum, in *Ultrasound, Its Chemical, Physical and Biological Effect*, edited by K.S. Suslick (VCH, New York, 1988), pp. 1–64.
19. A.L. Greer, *Science* **267**, 1947 (1995).
20. Yu. Koltypin, G. Kataby, X. Cao, R. Prozorov, and A. Gedanken, *J. Non-Cryst. Solids* **201**, 159 (1996).
21. K.V.P.M. Shafi, A. Gedanken, R.B. Goldfarb, and I. Felner, *J. Appl. Phys.* **81**, 6901 (1997).
22. K.V.P.M. Shafi, A. Gedanken, and R. Prozorov, *J. Mater. Chem.* **8**, 769 (1998).
23. X. Cao, R. Prozorov, Yu. Koltypin, G. Kataby, I. Felner, and A. Gedanken, *J. Mater. Res.* **12**, 402 (1997).
24. K.V.P.M. Shafi, Yu. Koltypin, A. Gedanken, R. Prozorov, J. Balogh, J. Lendvai, and I. Felner, *J. Phys. Chem. B.* **101**, 6409 (1997).
25. K.V.P.M. Shafi, R. Prozorov, J. Balogh, and A. Gedanken, *Chem. Mater.* **10**, 3445 (1998).
26. T. Pannaparayil, R. Marande, S. Komerneni, and S.G. Sankar, *J. Appl. Phys.* **64**, 5641 (1988).
27. X. Jiang, S.A. Stevenson, J.A. Dumesic, T.F. Kelly, and R.J. Casper, *J. Phys. Chem.* **88**, 6191 (1984).
28. N. Moumen and M.P. Pileni, *J. Phys. Chem.* **100**, 1867 (1996).
29. K.S. Suslick, T. Hyeon, and M. Fang, *Chem. Mater.* **8**, 2172 (1996).